TECHNICAL PAPER

Soft computing models for assessing bond performance of reinforcing bars in concrete at high temperatures

Asad S. Albostami[1,2] · Rwayda Kh. S. Al-Hamd[3] · Saif Alzabeebee[4]

Abstract

The bond between steel and concrete in reinforced concrete structures is a multifaceted and intricate phenomenon that plays a vital role in the design and overall performance of such structures. It refers to the adhesion and mechanical interlock between the steel reinforcement bars and the surrounding concrete matrix. Under elevated temperatures, the bond is more complex under higher temperatures, yet having an accurate estimate is an important factor in design. Therefore, this paper focuses on using data-driven models to explore the performance of the concrete-steel bond under high temperatures using a Gene Expression Programming (GEP) soft computing model. The GEP models are developed to simulate the bond performance in order to understand the effect of high temperatures on the concrete-steel bond. The results were compared to the multi-objective evolutionary polynomial regression analysis (MOGA-EPR) models for different input variables. The new model would help the designers with strength predictions of the bond in fire. The dataset used for the model was obtained from experiments conducted in a laboratory setting that gathered a 316-point database to investigate concrete bond strength at a range of temperatures and with different fibre contents. This study also investigates the impact of the different variables on the equation using sensitivity analysis. The results show that the GEP models are able to predict bond performance with different input variables accurately. This study provides a useful tool for engineers to better understand the concrete-steel bond behaviour under high temperatures and predict concrete-steel bond performance under high temperatures.

Keywords Concrete-Steel bond under High Temperatures · Gene Expression Programming · Soft computing

Introduction

Code standards like Eurocode 2 [1] and the CEB/FIB Model Code 2010 [2] offer ways to assess concrete behaviour for structural fire design. To maintain the structural integrity of reinforced concrete structures, attending to bond loss between steel–concrete during or after high temperatures exposure is essential. Standards have been developed to evaluate the bond strength between steel reinforcement and concrete after high-temperature exposure, including testing procedures such as pull-out tests or bond-slip tests. These standards may also recommend using fire-resistant materials and protective coatings to prevent or delay thermal degradation. By following these guidelines, reinforced concrete structures can maintain their load-carrying capacity even under fire conditions.

A reinforced concrete (RC) element's structural strength depends on the steel rebar and concrete bond strength. The steel–concrete bond is weakened when a reinforced concrete element is subjected to elevated temperatures. The leading

✉ Rwayda Kh. S. Al-Hamd
  r.al-hamd@abertay.ac.uk

  Asad S. Albostami
  asad.albostami@uop.edu.jo; asad.albostami@oryx.edu.qa

  Saif Alzabeebee
  Saif.Alzabeebee@qu.edu.iq

1 Civil Engineering Department, Faculty of Engineering, University of Petra, Amman, Jordan

2 School of Engineering & Construction, Oryx Universal College in Partnership with Liverpool John Moores, Doha, Qatar

3 School of Applied Sciences, Abertay University, Dundee, UK

4 Department of Roads and Transport Engineering, College of Engineering, University of Al-Qadisiyah, Al Diwaniyah, Al-Qadisiyah, Iraq

cause of this bond degradation is the weakening of the concrete, which causes the embedded steel rebar to bend plastically [3]. The decreased concrete-steel bond can greatly influence how RC components behave structurally since it changes how tensile stress is transferred [4]. Steel corrosion can damage the bond between steel and concrete components and impair their structural performance. Corrosion is another element that contributes substantially to the loss of bond strength [5].

In an attempt to uncover the key factors that affect performance and then create analytical correlations to predict bond strength, the influence of bond exposure to higher temperatures has been partially addressed in the literature [6–9]. Meanwhile, one of the least studied topics in concrete research is the bond between steel and concrete at high temperatures [10]. Furthermore, as the temperature rises, the bond between the concrete and steel may deteriorate, reducing the load that can be transferred between the two components. This may ultimately cause the reinforced concrete structure to crumble because of the C–S–H gel dehydration. Such dehydration can generate thermal spalling. To ensure the fire resistance of reinforced concrete structures and the safety of the people and property inside them, it is essential to understand how the bond between concrete and steel behaves under high temperatures [11]. Despite its significance, a study in this area of concrete science is still relatively underdeveloped.

Thermal spalling can be caused by various factors, including the heating rate of concrete [12], the mismatch in temperature and coefficients of thermal expansion between components [11, 13–17], and the explosive release of steam from the dehydration of C–S–H gel and portlandite [12], as well as CO_2 from calcined limestone aggregate. This particularly applies in situations where limestone aggregates are the dominant component. The manifestation of thermal spalling can have catastrophic effects on reinforced concrete structures [18], ultimately leading to their failure and putting lives and property at risk.

The amount of steel fibres in the concrete mix affects the temperature differential because the steel fibres, spread all through the concrete, disseminate heat considerably more quickly in the concrete [7]. Consideration of a range of variables is necessary when assessing the concrete performance in a structural component under elevated temperatures. These factors are concrete humidity, exposure time, temperature, aggregate type, peak temperature, member size, concrete age, the chemical composition of the cement, water-cement ratio (w/c), and loading conditions [3].

According to the literature, the primary factors influencing concrete-steel bond strength [6–9] are the altered compressive strength under elevated temperatures (f_c), the testing age of concrete (A), the concrete surface temperature at failure (T), thermal saturation ratio -the ratio of the duration of thermal saturation at the maximum target temperature to the minimum size of the pull-out specimen squared- (Δ), the ratio of the length-to-diameter ($\left(l/d\right)$) (i.e. the bond length of the embedded ribbed bar to the diameter of the bar), the cover-to-diameter ratio of the embedded ribbed bar to bar diameter ($\left(c/d\right)$), and finally, when using fibres, the total volume of fibre there is overall in the concrete (V).

The following analytical correlations have been developed by various researchers to anticipate the bond strength (T_b) at elevated temperatures. At this point, it should be emphasized that the available literature only contains a very small number of high-temperature correlations:

Yang et al. [5]	$T_b = \beta\sqrt{f_c(T)}$ Where β can be taken as 3.5 for $T = 20$ to 400 °C and as 2.5 for $T = 600$ to 800 °C	(1)
Varona et al. [6]	*For normal strength concrete;* $T_b = 0.354f_c - 0.15$	(2)
Varona et al. [6]	*For high strength concrete;* $T_b = 0.393f_c - 3.43$	(3)

The relationships described in this context were established using traditional regression analysis. However, the current Eurocode approach relies on parameters to simulate different bond conditions, using a simplified estimate based on the tensile strength of concrete. Structural engineers are now recognizing the value of artificial intelligence (AI) and machine learning (ML) advancements, which offer the potential for improved design guidance [19]. In civil engineering disciplines like hydraulic, geotechnical, and structural engineering, these AI and ML approaches have shown enhanced accuracy compared to existing methods [20–30]. They provide new perspectives and practical solutions for accelerating innovations in the design and development of cementitious materials. By utilizing data-driven models and existing datasets, ML can automatically identify patterns and extract valuable information, accounting for the complex nature of concrete mixtures and their properties [31]. ML is being utilized as a powerful tool to establish relationships between processes, structures, properties, and performance. It aids in identifying cement hydration and concrete degradation mechanisms, assisting in concrete materials design, and facilitating high-throughput experimentation and computation. ML has been explored in various concrete applications, including cement pastes, mortars, and different types of concrete such as high-performance concrete, self-consolidating concrete, reinforced concrete, recycled aggregate concrete, lightweight aggregate concrete, alkali-activated concrete, and 3D-printed concrete [32–40].

The transformative potential of ML in concrete research is evident due to its capability to handle complex tasks autonomously. However, to fully harness the benefits of ML

for concrete mixture design, it is essential to understand the methodological limitations and establish best practices in this emerging computational field. Reference [41] focuses on the positive impacts of ML in concrete science, discussing its implementation, application, and interpretation of algorithms. Additionally, it outlines future directions for the concrete community to maximize the potential of ML models.

A recent study by Al-Hamd et al. [42] addresses employing a progressive regression analysis approach to bond strength. This technique uses the multi-objective evolutionary polynomial regression analysis (MOGA-EPR) in predicting bond strength and yields a highly accurate estimation. In this study, the three correlations expressly as shown in Table 1 (Eqs. 4 to 6) to predict bond strength (T_b) take into account all the essential variables and produce more precise correlations. When developing the correlation, its practicability was also taken into account. The correlations discussed include all the variables found in the first MOGA-EPR correlation model (1). Then for the second and the third MOGA-EPR correlation models (2) and (3), respectively eliminating the thermal saturation ratio (Δ) and the testing age of concrete (A), respectively (as shown in Table 2) as it is difficult to obtain these experimentally. Table 2 summarizes the included and excluded input variables for the development of the models. The input variables as shown in Tables 1 and 2 (Eqs. 4, 5 and 6) were used in the development of the process that predicts the correlation of the bond strength (T_b) in MPa are (f_c) in MPa; (A) in days; (V); (Δ); (l/d) and (c/d).

When it comes to Artificial Intelligence (AI) and Machine Learning (ML), the Gene Expression Programming (GEP) algorithm is an improved version of Genetic Programming (GP) [43], and it is used in civil engineering disciplines to provide more accurate predictions than existing approaches [44]. This approach has been proven to be successful in modelling intricate and nonlinear procedures [44]. This research paper takes advantage of GEP to develop a novel application for this method to the concrete-steel bond strength (T_b). Individuals are encoded in the form of linear chromosomes of uniform lengths that can be expressed as tree structures [43]. Mutation and recombination, which are genetic operators, can be implemented on the linear structure of the chromosomes, thereby generating legitimate and accurate structures for solutions.

This research conducted here is based on 316 previous tests (Varona et al. [6]). To predict the concrete-steel bond strength (T_b) under high temperatures, various models have been designed using the GEP approach, and then compared with the Multi-Objective Genetic Algorithm Evolutionary Polynomial Regression (MOGA-EPR) models developed by Al Hamad et al. [42]. Following validation and comparison of the different models, novel sensitivity studies were conducted to investigate the effect of altering some of the input variables without the requirement for more experiments.

Table 2 The input variables

Correlation #	Included variables	Excluded variables
Correlation (1)	$f_c, A, V, \Delta, l/d$ and c/d	None
Correlation (2)	$f_c, A, V, l/d$ and c/d	Δ
Correlation (3)	$f_c, V, l/d$ and c/d	A and Δ

Table 1 MOGA-EPR Correlation Equations [42]

| MOGA-EPR correlation # [42]	MOGA-EPR correlation equation	Coefficients	Equation #
MOGA-EPR Correlation model (1)	$$T_{batfailure} = a_1 \times \sqrt{c/d} \times \sqrt{A} \times f_c \\ + a_2 \times c/d \times f_c \times T^2 + a_3 \times \sqrt{l/d} \times \sqrt{A} \times f_c \\ + a_4 \times \sqrt{V} \times \sqrt{\Delta} \times (c/d) \times T^2 \\ + a_5 \times \sqrt{l/d} \times \sqrt{V} \times (c/d) + a_6$$	$a_1 = 3.59 \times 10^{-2}$ $a_2 = -7.5 \times 10^{-8}$ $a_3 = -1.68 \times 10^{-2}$ $a_4 = -3.5 \times 10^{-6}$ $a_5 = 8.48 \times 10^{-1}$ $a_6 = 4.047$	(4)
MOGA-EPR Correlation model (2)	$$T_{batfailure} = b_1 \times c/d \times f_c \times T^2 \\ + b_2 \times c/d \times f_c \times \sqrt{A} + b_3 \times (c/d)^2 \times f_c^2 \times \sqrt{A} \\ + b_4 \times \sqrt{l/d} \times \sqrt{c/d} \times \sqrt{A} \times f_c + b_5 \times V \times f_c \times (c/d)^2 + b_6$$	$b_1 = -1.12 \times 10^{-7}$ $b_2 = 2.3 \times 10^{-2}$ $b_3 = -1.8 \times 10^{-5}$ $b_4 = -8.7 \times 10^{-3}$ $b_5 = 1.05 \times 10^{-2}$ $b_6 = 2.789$	(5)
MOGA-EPR Correlation model (3)	$$T_{batfailure} = c_1 \times f_c + c_2 \times \sqrt{c/d} \times \sqrt{f_c} \times T^2 \\ + c_3 \times \sqrt{l/d} \times f_c + c_4 \times l/d \times \sqrt{c/d} \times f_c \\ + c_5 \times \sqrt{V} \times \sqrt{f_c} \times l/d \times (c/d)^2 + c_6$$	$c_1 = 6.926 \times 10^{-1}$ $c_2 = -1.21 \times 10^{-6}$ $c_3 = -3.08 \times 10^{-1}$ $c_4 = 1.5 \times 10^{-2}$ $c_5 = 1.47 \times 10^{-2}$ $c_6 = 6.224$	(6)
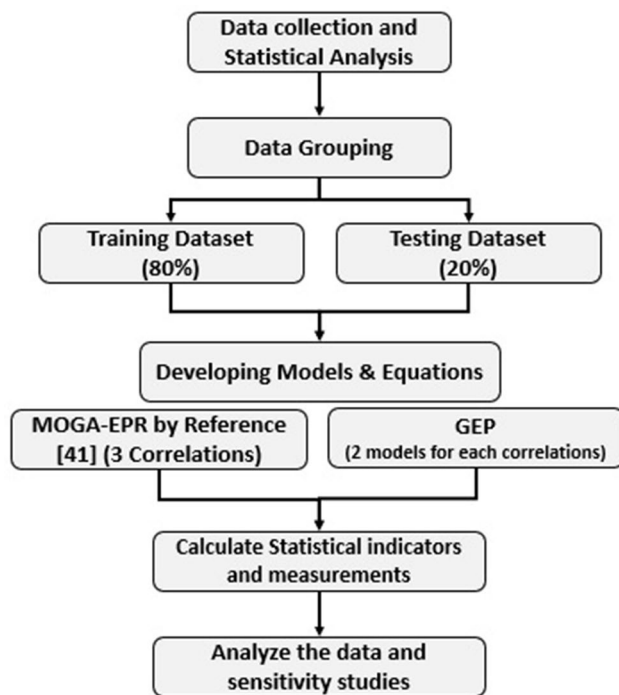
Fig. 1 Flowchart process for this paper methodology

Methodology

This paper explores the possibility of predicting the correlation of bond strength (T_b) of reinforcing bars in concrete exposed to high temperatures using an innovative GEP model. It is compared to the MOGA-EPR model proposed by Al Hamad et al. [42]. The experimental database created from existing literature (Varona et al. [9]) is used to train and evaluate the T_b.

A flowchart (Fig. 1) is presented to illustrate the steps followed in this study. Beginning with the collection and statistical analysis of the data, the process continued with the grouping of the data, the development of models and GEP model equations, the calculation of statistical indicators, the analysis of the results, and the running of sensitivity studies to evaluate the influence of critical input variables on T_b.

Data collection and statistical analysis

Varona et al. [9] compiled a 316-point database to investigate concrete bond strength at a range of temperatures and with different fibre contents. Using the data from their database and a review of previous studies [6–9], they developed analytical regression correlations determined by the significant parameters impacting the bond strength (T_b) at ambient or high temperatures. Varona et al.'s data [9] used in this work are provided in Table 3.

Data grouping

This study evaluated the performance of two Gene Expression Programming (GEP) models in comparison to a Multi-Objective Genetic Algorithm Evolutionary Polynomial Regression (MOGA-EPR) model as proposed by Al Hamad et al. [42], for predicting bond strength (T_b). The collected data was divided into two sets to ensure accuracy: 80% for training the models and 20% for testing. The statistical measures pertinent to the training and testing datasets are presented in Tables 4 and 5.

Developing the GEP models

In this paper, GEP analysis was conducted using the GeneXproTools software [45]. Firstly, chromosomes are basic elements: they are linear, condensed, relatively small, and easily modifiable through genetic methods (such as replication, mutation, recombination, and transposition). Secondly, the chromosomes were then presented as tree expressions; this is the subject of selection, and according to the fitness, the chromosomes are chosen to reproduce and be modified. During reproduction, it is the chromosomes, not the expression trees, that are modified and passed on to the next generation [46].

Table 3 Statistical measures of the measured data [9]

Statistical measure/Variable	Minimum	Maximum	Mean	Standard deviation
Fibre volume fraction (V) (%)	0.00	2.00	0.15	0.45
Length to diameter (l/d)	2.00	20.83	9.74	6.04
Cover to diameter (c/d)	1.78	5.75	4.64	1.26
Age at testing (A) (days)	28.00	90.00	43.78	23.41
Δ (h/dm^2)	0.33	3.00	1.82	1.04
Failure surface temperature of concrete (T) (°C)	20.00	825.00	347.74	250.02
$f_{c(cube)}$ at 20 C°(MPa)	0.38	103.60	31.74	17.76
T_b, at failure °C (MPa)	1.06	36.30	8.41	6.27

Table 4 Statistical measures of the training dataset

Statistical measure/Variable	Minimum	Maximum	Mean	Standard deviation
Fibre volume fraction (V) (%)	0.00	2.00	0.16	0.48
Length to diameter (l/d)	2.00	20.83	9.66	6.03
Cover to diameter (c/d)	1.78	5.75	4.58	1.28
Age at testing (A) (days)	28.00	90.00	43.64	23.39
Δ (h/dm^2)	0.33	3.00	1.82	1.03
Failure surface temperature of concrete (T) (°C)	20.00	825.00	342.15	250.17
$f_{c(cube)}$ at 20 °C (MPa)	0.38	103.60	32.29	18.37
T_b, at failure °C (MPa)	1.06	36.30	8.49	6.36

Table 5 Statistical measures of the testing dataset

Statistical measure/Variable	Minimum	Maximum	Mean	Standard deviation
Fibre volume fraction (V) (%)	0.00	2.00	0.08	0.26
Length to diameter (l/d)	2.00	20.83	10.06	6.12
Cover to diameter (c/d)	1.78	5.75	4.86	1.13
Age at testing (A) (days)	28.00	90.00	44.37	23.63
Δ (h/dm^2)	0.33	3.00	1.82	1.08
Failure surface temperature of concrete (T) (C°)	20.00	825.00	370.38	249.74
$f_{c(cube)}$ at 20 °C (MPa)	5.10	81.70	29.52	14.97
T_b, at failure °C (MPa)	1.07	29.40	8.06	5.89

Reproduction encompasses much more than simply replicating genetic material; genetic operators are also integral to creating genetic diversity. Replication allows for the transmission of the genome to the subsequent generation. Nonetheless, replication alone does not introduce new genetic variation; this is only achievable through the operation of the other genetic operators. These operators randomly select the chromosomes to be changed, so in Genetic Expression Programming (GEP), a chromosome may be altered by one or more operators, or remain unaltered. Figure 2 shows the flowchart of GEP.

The parameters commonly used in GEP include chromosome length, gene set, head length, tail length, population size, crossover and mutation rates, and selection strategy. The chromosome length determines the number of genes in a chromosome, affecting the complexity and size of the evolved programs. The gene set represents the available genes used to construct the chromosomes, including functions and terminals specific to the problem domain [43, 47].

The head length parameter determines the size of the main program structure within the chromosome, while the tail length parameter controls the size of the tail region, providing additional genetic material for variation. The population size refers to the number of individuals in each generation and influences the exploration of the search space. The crossover and mutation rates determine the probabilities of genetic material exchange and random changes
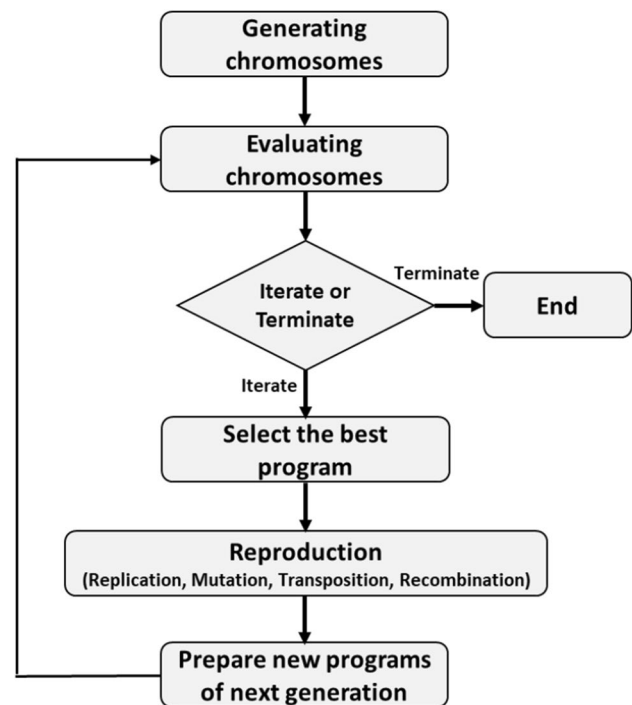
Fig. 2 The flowchart of a GEP algorithm

in individuals, respectively. Finally, the selection strategy determines how individuals are chosen for the next generation from the current population [43, 47].

Symbolic regression or function finding stands out as a significant application of GEP parameters. Its objective is to discover an expression that performs effectively across all fitness cases, allowing for a permissible error from the correct value. In certain mathematical scenarios, it proves advantageous to use small relative or absolute errors in order to reveal highly optimal solutions. However, if the selection range is excessively narrow, populations evolve slowly and encounter difficulties in finding the correct solution. On the other hand, if the selection range is overly broad, numerous solutions with maximum fitness may emerge, but they are likely to be far from satisfactory solutions [43, 47].

Another parameter to consider is the mutation rate. Mutations have the potential to occur at any position within the chromosome. Nonetheless, it is crucial to maintain the structural organization of the chromosomes. In the head section, any symbol can be transformed into another symbol, whether it is a function or a terminal. Conversely, in the tail section, only terminals can change into other terminals. Adhering to these guidelines ensures the preservation of the chromosomes' structural integrity, guaranteeing that all newly generated individuals resulting from mutations are valid programs that maintain structural accuracy. Typically, a mutation rate equivalent to two-point mutations per chromosome is commonly utilized [43, 47].

These parameters are typically set by the user based on the specific problem domain, the complexity of the task, and the available computational resources. Proper parameter tuning is crucial to achieving good performance and efficient convergence in GEP. Different combinations of parameter values can have a significant impact on the search process and the quality of the evolved solutions. Therefore, experimentation and fine-tuning of parameters are often necessary to obtain optimal results.

In this paper, six GEP models were established, with two models that compared each of the MOGA-EPR correlation equations. The input variables relevant to the correlations have been discussed in Sect. "Introduction" and Table 2. Two different GEP models were developed for each correlation criterion, one using the fundamental operations $(+, -, \times$ and $/)$ and the other including the square root function. Both models were then pitted against the MOGA-EPR models to identify the most accurate one.

Correlation (1) models

In these correlation models, all of the input variables (f_c, A, V, Δ, l/d and c/d) are listed in Table 2 and have been

included in the correlation model equations to predict the T_b values.

Tables 6 and 7 report the main setting parameters and the developed equations of the GEP models. In Table 6, the changing of head sizes and/or a number of gene values is to get the most accurate and higher precise equations and models.

Correlation (2) models

In these correlation models, the five input parameters (f_c, A, V, l/d and c/d) are used in the equations shown in Table 2 to calculate the T_b values.

Tables 8 and 9 report the main setting parameters and the developed equations of the GEP models.

Correlation (3) models

In t correlation models, the input variables (f_c, V, l/d and c/d) are included in the model equations for predicting the T_b values as mentioned in Table 2.

Tables 10 and 11 report the main setting parameters and the developed equations of the GEP models.

In the following section, the statistical metrics for the various models will be calculated and discussed, and the findings from the models will be contrasted.

Statistical indicators and measurements

Utilizing statistical measures, including mean absolute error (MAE), root mean square error (RMSE), mean (μ), and coefficient of determination (R^2), the effectiveness of the new and old analytical techniques was evaluated (Eqs. 13–16). Multiple earlier studies have employed this similar accuracy assessment technique [48–52]. The MAE and RMSE values identify the lower means as the ideal match. The optimal value for the

Table 6 The main setting parameters and adjustments of GEP models for Correlation (1)

GEP parameter	Setting of parameters	
	Model (1)	Model (2)
Number of chromosomes	30	30
Head size	9	10
Number of genes	5	5
Function set	$+, -, \times$ and $/$	$+, -, \times, /$ and $\sqrt{}$
Fitness function	RMSE	RMSE
Mutation rate	0.00138	0.00138
Inversion rate	0.00546	0.00546
Gene transposition rate	0.00277	0.00277
Random chromosomes	0.0026	0.0026
Gene recombination rate	0.00277	0.00277

Table 7 GEP models equations for Correlation (1)

Model #	Predicted T_b equation	Coefficients	Equation #
Model (1)	$$T_{batfailure} = \frac{(2c/d)+d_1+f_c+\Delta}{l/d-V} + \frac{(d_2+l/d)l/d+T+d_3}{f_c+l/d-(A\times l/d)}$$ $$+ c/d + d_4 + 1 + \frac{V\times(c/d-\Delta+d_5)}{\Delta} + \frac{f_c}{(((d_6\times d_7)-\frac{\Delta}{T})-T)\times c/d}$$	$d_1 = -4.02133388560114$ $d_2 = -9.83520004882961$ $d_3 = -11.3166343688427$ $d_4 = -2.0533661915952$ $d_5 = 0.490860314807632$ $d_6 = -1.95675110452493$ $d_7 = -7.4492222178347$	(7)
Model (2)	$$T_{batfailure} = V + \sqrt{\frac{(A\times c/d)+A-e_1}{(2c/d+A-l/d)}} + e_2$$ $$+ \frac{c/d}{\left(e_2-\left(\frac{V\times l/d}{\Delta}\right)\right)\times e_2} + \frac{(2A-l/d-T)\times\sqrt{2f_c}}{l/d\times A^{1.5}} + e_3 + \sqrt{\frac{(V+e_4)}{(l/d+e_5)}}\times f_c\times c/d$$	$e_1 = -2.82162236396374$ $e_2 = 3.15728608325765$ $e_3 = -7.44591314471175$ $e_4 = 5.85987746785495$ $e_5 = -0.248122964310291$	(8)

Table 8 The main setting parameters and adjustments of GEP models for Correlation (2)

GEP parameter	Setting of parameters	
	Model (3)	Model (4)
Number of chromosomes	30	30
Head size	9	9
Number of genes	4	5
Function set	$+,-,\times$ and $/$	$+,-,\times,/$ and $\sqrt{}$
Fitness function	RMSE	RMSE
Mutation rate	0.00138	0.00138
Inversion rate	0.00546	0.00546
Gene transposition rate	0.00277	0.00277
Random chromosomes	0.0026	0.0026
Gene recombination rate	0.00277	0.00277

parameter μ is 1.0; values below this suggest a general underprediction of the bond strength, and values above imply a general overprediction.

$$MAE = \frac{1}{n}\sum_{1}^{n}\left|T_{b,p} - T_{b,m}\right| \tag{13}$$

$$RMSE = \sqrt{\frac{1}{n}\sum_{1}^{n}\left(T_{b,p} - T_{b,m}\right)^2} \tag{14}$$

$$Mean(\mu) = \frac{1}{n}\sum_{1}^{n}\left(\frac{T_{b,p}}{T_{b,m}}\right) \tag{15}$$

Table 9 GEP models equations for Correlation (2)

Model #	Predicted T_b equation	Coefficients	Equation #
Model (3)	$$T_{batfailure} = ((c/d - f_1 - \frac{c/d\times(f_2-A)}{T})\times V) + (\frac{f_3\times c/d}{T} - \frac{l/d-f_c}{f_4+l/d} - f_5)$$ $$+ \frac{f_c}{\left(\frac{c/d\times(T-A)}{f_6+f_7}\right)+V} + c/d + \frac{c/d}{\left(\frac{c/d\times A}{T}\right)+V-f_c}$$	$f_1 = 1.31835418556042$ $f_2 = 14.369181508319$ $f_3 = 14.6889216995212$ $f_4 = 0.133214111144357$ $f_5 = 1.24768634441483$ $f_6 = 1.95134120236163$ $f_7 = -0.015062690634106$	(9)
Model (4)	$$T_{batfailure} = c/d + (\frac{(g_1-V-\frac{f_c}{c/d})}{A-T}) + g_2 + (V\times(\frac{(g_3\times V)-(g_4\times g_5)+A}{g_6}))$$ $$+ g_7 + (\frac{(g_8+\frac{f_c}{g_7})}{(A\times V)+g_9-T}) + \frac{f_c}{l/d} + \frac{c/d}{\sqrt{T}\times\sqrt{g_{10}}} + g_{11} - V^{0.125}$$	$g_1 = -7.04458754234443$ $g_2 = -6.13703152280304$ $g_3 = -11.8357151889437$ $g_4 = 8.90229224524674$ $g_5 = 0.0439399194616535$ $g_6 = 6.12652730320557$ $g_7 = 7.01989888605853$ $g_8 = 0.871456941078571$ $g_9 = 0.343772233305734$ $g_{10} = 0.0499310267595848$ $g_{11} = -4.52339457380902$	(10)

Table 10 The main setting parameters and adjustments of GEP models for Correlation (3)

GEP parameter	Setting of parameters	
	Model (5)	Model (6)
Number of chromosomes	30	30
Head size	10	9
Number of genes	6	6
Function set	$+, -, \times$ and $/$	$+, -, \times, /$ and $\sqrt{}$
Fitness function	RMSE	RMSE
Mutation rate	0.00138	0.00138
Inversion rate	0.00546	0.00546
Gene transposition rate	0.00277	0.00277
Random chromosomes	0.0026	0.0026
Gene recombination rate	0.00277	0.00277

$$R^2 = \left(\frac{\sum_{i=1}^{n}(T_{b,p} - T_{b,p_{average}})(T_{b,m} - T_{b,m_{average}})}{\sqrt{\sum_{i=1}^{n}(T_{b,p} - T_{b,p_{average}})^2 \sum_{i=1}^{n}(T_{b,m} - T_{b,m_{average}})^2}} \right)^2 \tag{16}$$

In Eqs. (13)–(16), the term 'n' stands for the amount of data points taken into account when assessing the bond strength (T_b), with '$T_{b,p}$' representing the predicted bond strength, and '$T_{b,m}$' denoting the measured bond strength.

Results

Correlation (1) results

Table 12 and Fig. 3 demonstrate the calculation of the mean absolute error (MAE), root mean squared error (RMSE),

Table 11 GEP models equations for Correlation (3)

Model #	Predicted T_b equation	Coefficients	Equation #
Model (5)	$T_{batfailure} = c/d + h_1 + (\frac{h_2}{h_3} \times \frac{V}{T} \times (T - l/d)) + \frac{(c/d + f_c - \frac{f_c}{c/d}) \times (\frac{c/d}{l/d} + c/d)}{(c/d \times l/d) - V - h_4}$ $+ 2h_5 + (\frac{c/d^2 \times V}{T} \times (c/d + h_6)) + \frac{T}{(h_7 + l/d) \times (h_8 - V) \times (h_9 \times c/d^2)} + \frac{h_{10} - T - 2c/d}{h_{11} - c/d - c/d^2}$	$h_1 = 6.72220138634907$ $h_2 = -9.83733063127537$ $h_3 = -8.96069493697928$ $h_4 = 2.36795561174352$ $h_5 = -3.31615874279132$ $h_6 = -9.81580553605762$ $h_7 = -3.49237127774238$ $h_8 = -8.07519140742794$ $h_9 = -3.64402905362102$ $h_{10} = 9.94811416994824$ $h_{11} = 210.77762807679$	(11)
Model (6)	$T_{batfailure} = i_1 + i_2 + \frac{(V \times i_3) + c/d}{T} + \frac{f_c + l/d}{\sqrt{l/d + \frac{l/d}{c/d} - \frac{l/d}{i_4}}}$ $+ c/d + T^{0.25} + \frac{V + i_5}{l/d} - i_6^{\,2} + \frac{c/d \times i_7}{V - T} + \frac{i_7 - l/d}{i_7 + T} + \sqrt{V} + i_8 + i_9$ $- \sqrt{\frac{V}{l/d + i_{10}}} + \sqrt{V \times ((V^2 \times i_{11}) + c/d - i_{12} - i_{13})}$	$i_1 = -8.66739483341553$ $i_2 = 6.78827639161741$ $i_3 = 11.0884557268852$ $i_4 = -2.6891296133704$ $i_5 = 7.06379962700155$ $i_6 = 2.84970681621856$ $i_7 = -13.2372635780051$ $i_8 = 8.70957760019792$ $i_9 = 1.34619806244417$ $i_{10} = -3.31755092909635$ $i_{11} = -4.72811151789992$ $i_{12} = -9.98118039223781$ $i_{13} = -8.65689695633331$	(12)

Table 12 Statistical measures of the testing and training datasets for Correlation (1)

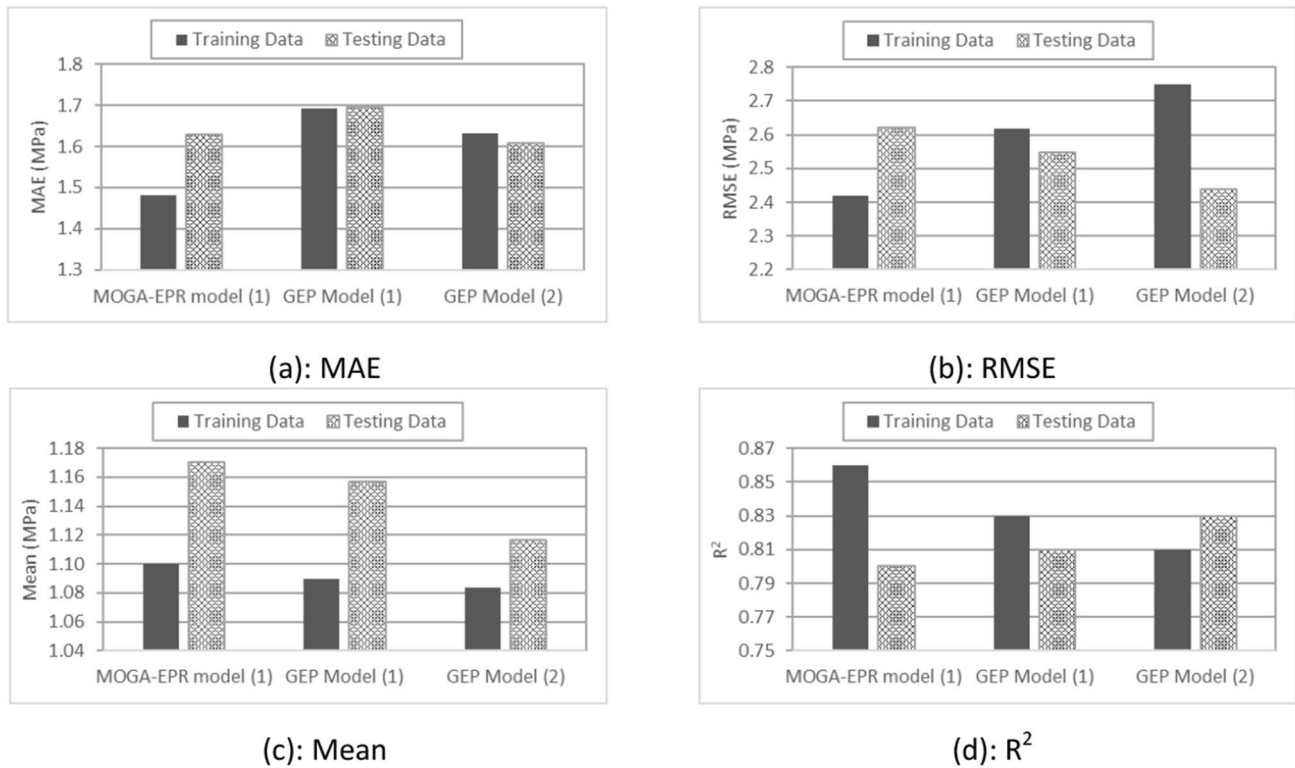| Statistical indicators	Training data			Testing data		
	MOGA-EPR correlation (1)	GEP model (1)	GEP model (2)	MOGA-EPR correlation (1)	GEP model (1)	GEP model (2)
MAE (MPa)	1.48	1.69	1.63	1.63	1.70	1.61
RMSE (MPa)	2.42	2.62	2.75	2.62	2.55	2.44
Mean (μ)	1.10	1.09	1.08	1.17	1.16	1.12
R^2	0.86	0.83	0.81	0.80	0.81	0.83

(a): MAE

(b): RMSE

(c): Mean

(d): R^2

Fig. 3 The Statistical indicators of the developed models for both datasets for Correlation (1)

mean (μ), and coefficient of determination (R^2) for the prediction of bond strength (T_b), compared to the measured T_b for the training and testing datasets for each correlation model of the MOGA-EPR and GEP techniques based on the statistical indicators and measurements in Eqs. (13)–(16). The results from Table 9 and Fig. 3 for correlation (1) models indicate:

- MAE for GEP models (1) and (2) from training datasets is between 1.63 and 1.69, and from testing datasets, it is between 1.61 and 1.70.
- RMSE from training datasets ranges from 2.62 to 2.75, and RMSE from testing datasets ranges from 2.44 to 2.55.
- The mean of the datasets from training datasets is between 1.08 and 1.09, and from testing datasets is between 1.12 and 1.16.
- R^2 scores from both training and testing datasets are between 0.81 and 0.83.

The comparison of the MOGA-EPR statistical indicators to the ones calculated by the GEP technique for the training and testing datasets from Table 12 and Fig. 3 is promising and relatively consistent. The MOGA-EPR model has the most impressive R^2 for the training dataset when compared to the two GEP models, with the GEP model (1) having a

Table 13 Statistical measures of all datasets for Correlation (1)

Statistical measure/ Approach	MOGA-EPR Correlation (1)	GEP model (1)	GEP model (2)
MAE (MPa)	1.51	1.69	1.63
RMSE (MPa)	2.46	2.60	2.69
Mean (μ)	1.11	1.10	1.09
R^2	0.85	0.83	0.82

higher R^2 than the GEP model (2). Additionally, for the testing datasets, the GEP model (2) has a higher R^2 than both MOGA-EPS and the GEP model (1). MOGA-EPR also has the lowest MAE and RMSE values of all the models, and the mean values are all close to 1.

Table 13 and Fig. 4 compare the statistical indicators of correlation between the MOGA-EPR and GEP models for all datasets. It is evident that the GEP model (1) is more proximate to the MOGA-EPR model than the GEP model (2). Additionally, the MOGA-EPR model demonstrates a greater degree of accuracy in its correlation with R^2 in predicting the T_b than the GEP models. Despite this fact, the GEP models produce results that are quite similar to those of the MOGA-ERP.

(a): MAE

(b): RMSE

(c): Mean

(d): R²
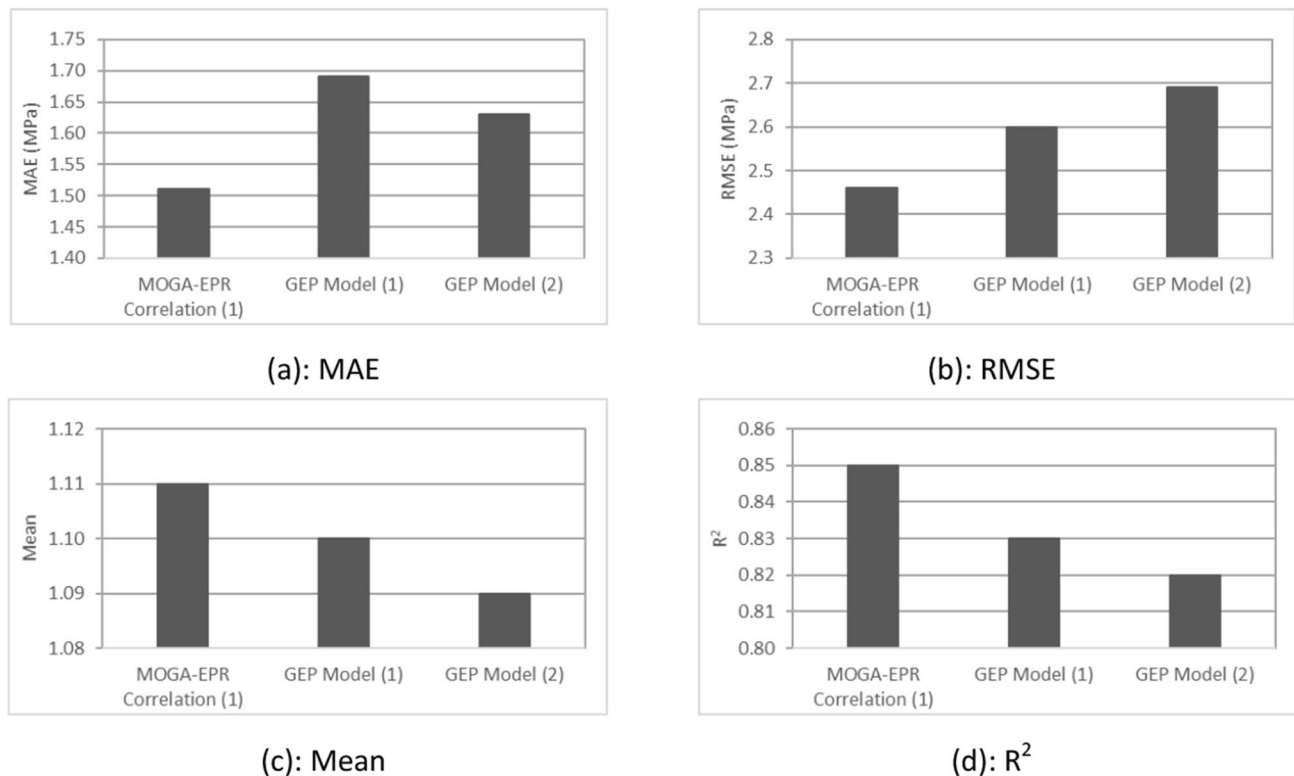
Fig. 4 The Statistical indicators of the MOGA-EPR and developed models for all datasets for Correlation (1)

As shown in Table 14, the GEP-developed models for correlation (1) appear to have accurately predicted the measured T_b. Most of the predictions made by these models are close to the perfect fit line and remain within the $\pm 30\%$ error margin. This implies that the models have performed adequately.

Correlation (2) Results

For Correlation (2), thermal saturation ratio, (Δ) is excluded in developing the models, due to the difficulty to measure this factor expectantly [42].

Table 15 and Fig. 5 present a comparison of the mean absolute error (MAE), root mean squared error (RMSE), mean (μ), and coefficient of determination (R^2) for the prediction of bond strength (T_b) using the MOGA-EPR and GEP techniques for both the training and testing datasets of the correlation (2) models. The analysis of the correlation models in this table and figure indicates that the GEP models (3) and (4) yielded MAE values between 1.60 and 1.65 from the training datasets, and from the testing datasets, the MAE values are between 1.76 and 1.79. The RMSE from the training datasets ranged from 2.54 to 2.56, and the RMSE testing datasets ranged from 2.94 to 3.09. The mean of the datasets from the training datasets is 1.09, and the mean of the datasets from testing datasets is between 1.15 and 1.17.

The R^2 score from the training datasets is 0.84, and from the testing datasets, it is between 0.72 and 0.75.

Comparing Table 16 and Fig. 6, it is clear that the GEP models are close to the MOGA-EPR model in terms of statistical indicators of correlation. Nevertheless, the MOGA-EPR model shows more precision in its correlation with the R^2 value when predicting T_b than the GEP models. Even though the GEP models are slightly less accurate than the MOGA-EPR model, their results are still relatively close to those of the MOGA-ERP.

The GEP-created models for Correlation (2) seem to have accurately estimated the measured T_b, similar to Correlation (1) demonstrated in Table 17. Most of the models' predictions fall close to the exact fit line and are within the $\pm 30\%$ error limit. This implies that the models have worked satisfactorily.

Correlation (3) results

The models developed for Correlation (3) exclude the thermal saturation ratio (Δ) and the total overall volume of fibre overall in the concrete (V) because it is challenging to measure these factors accurately [42]. Table 18 and Fig. 7 demonstrate a comparison of the mean absolute error (MAE), root mean squared error (RMSE), mean (μ) and coefficient of determination (R^2) for the prediction of bond strength

Table 14 Relationship between measured and predicted T_b in MPa using the GEP-developed models for the training and testing datasets for Correlation (1)

GEP model #	Training dataset	Testing dataset
Model (1)		
Model (2)		
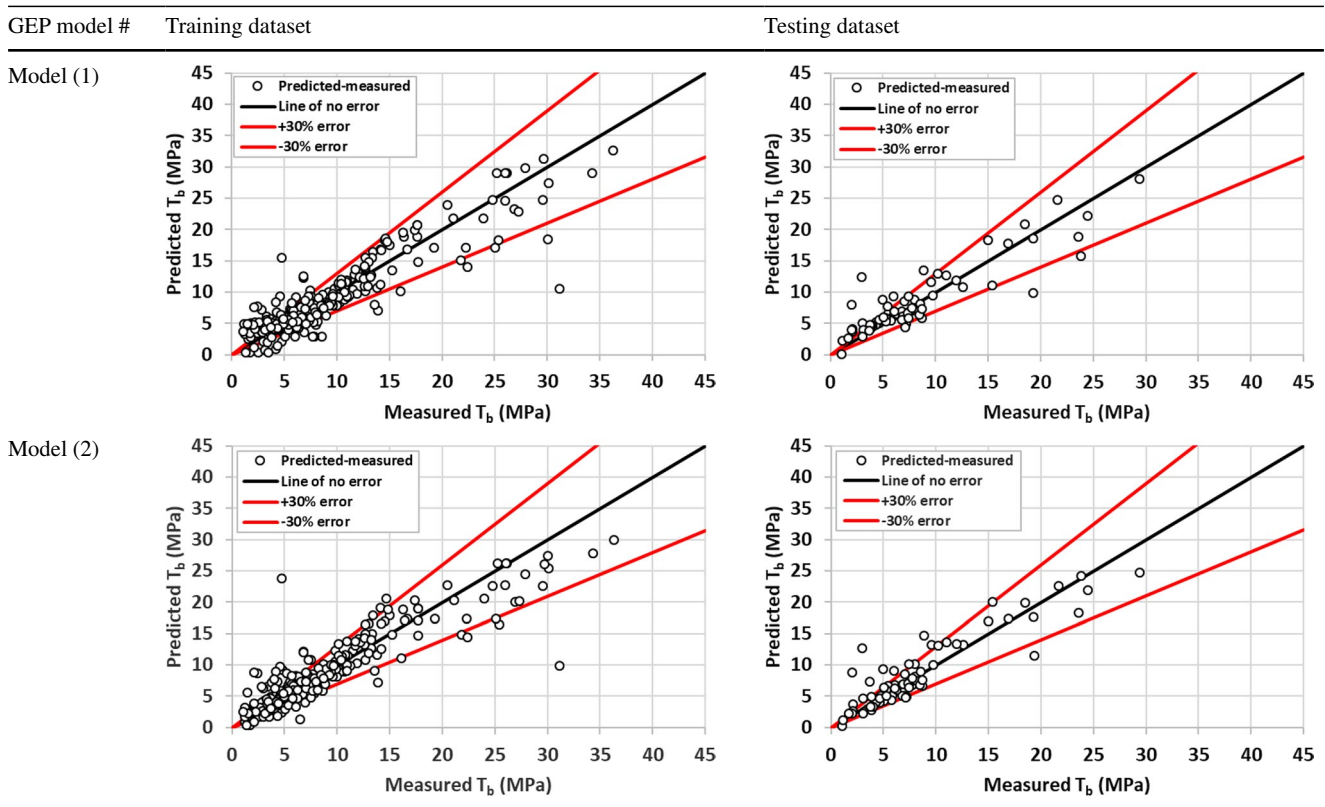
(T_b) using the MOGA-EPR and GEP techniques for both the training and testing datasets of correlation (3) models. The results of this comparison show that the GEP models (5) and (6) yielded MAE values from the training datasets between 1.51 and 1.82, and the testing datasets between 1.61 and 1.78. The RMSE from the training datasets is in the range of 2.40 to 2.88 and from the testing datasets between 2.71 to 2.99. The mean of the datasets from the training datasets is between 1.05 and 1.12, and from the testing datasets between 1.10 and 1.14. The R^2 scores from the training datasets are in the range of 0.86 to 0.80 and from the testing datasets between 0.74 and 0.79.

Based on Table 19 and Fig. 8, the GEP model (5) demonstrates a greater degree of accuracy in its correlation with R^2 in predicting the Tb than the MOGA-EPR model (3).

Similar to Correlations (1 and 2), the GEP-created models for Correlation (3) seem to have accurately estimated the measured T_b as demonstrated in Table 20. Most of the models' predictions fall close to the exact fit line and are within the ± 30% error limit. This implies that the models have worked satisfactorily.

Table 15 Statistical measures of the testing and training datasets for Correlation (2)

Statistical indicators	Training data			Testing data		
	MOGA-EPR Correlation (2)	GEP model (3)	GEP model (4)	MOGA-EPR correlation (2)	GEP model (3)	GEP model (4)
MAE (MPa)	1.54	1.60	1.65	1.70	1.79	1.76
RMSE (MPa)	2.39	2.56	2.54	2.51	3.09	2.94
Mean (μ)	1.06	1.09	1.09	1.13	1.17	1.15
R^2	0.86	0.84	0.84	0.82	0.72	0.75

(a): MAE
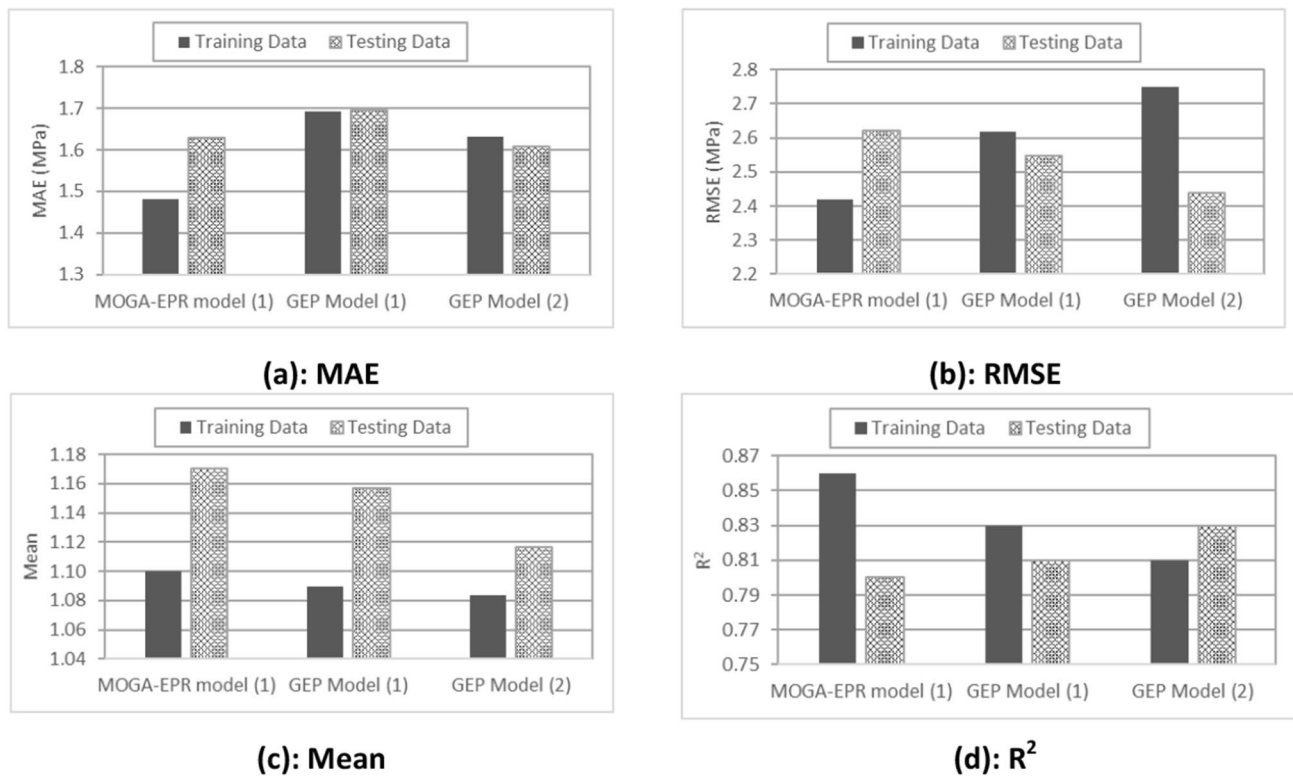

(b): RMSE

(c): Mean

(d): R²

Fig. 5 The Statistical indicators of the developed models for both datasets for Correlation (2)

Table 16 Statistical measures of all datasets for Correlation (1)

Statistical measure/ Approach	MOGA-EPR correlation (2)	GEP model (3)	GEP model (4)
MAE (MPa)	1.57	1.64	1.67
RMSE (MPa)	2.41	2.67	2.62
Mean (μ)	1.07	1.11	1.10
R^2	0.85	0.82	0.82

Sensitivity studies

After analysing the T_b values from different models in the previous sections, the MOGA-EPR and GEP model (5) were chosen to perform additional sensitivity studies for correlations (1) and (3) respectively. The two models were picked because of their simplicity and higher R^2 values, thus, they could be used to conduct a sensitivity analysis of the parameters influencing T_b. These studies will show how changing the values of the input variables impacts T_b.

This paper has already presented more accurate prediction models. Because Δ and A are hard to measure in real-life experiments, the models are beneficial in predicting the effect of changing these factors on T_b without needing to measure them experimentally. Consequently, Figs. 9a, b analyse the effect of altering these factors on T_b.

In Fig. 9a, it can be seen that as the thermal saturation ratio (Δ) increases, the bond between steel rebar and concrete (T_b) decreases. This trend can be due to thermally induced stress. When the thermal saturation ratio is increased, the steel rebar can expand more due to the increased heat, which creates more tension in the bond between the steel rebar and concrete. This tension can lead to a decrease in the bond strength between the two materials, thus decreasing the T_b value.

As shown in Fig. 9b, this study examines the effect of changing the Age of Testing (A) on the Concrete-Steel Bond Performance under High Temperatures. The result shows that there is an increasing relation between A and bond performance–meaning that as A increases, the bond performance also increases.

Increasing the age of testing (A) on the concrete-steel bond performance under high temperatures increases the bond performance because aging increases the bond strength between the concrete and steel due to the formation of additional strong chemical bonds between the concrete and steel. Aging also increases the porosity of the concrete, which increases the surface area available for bond formation. The
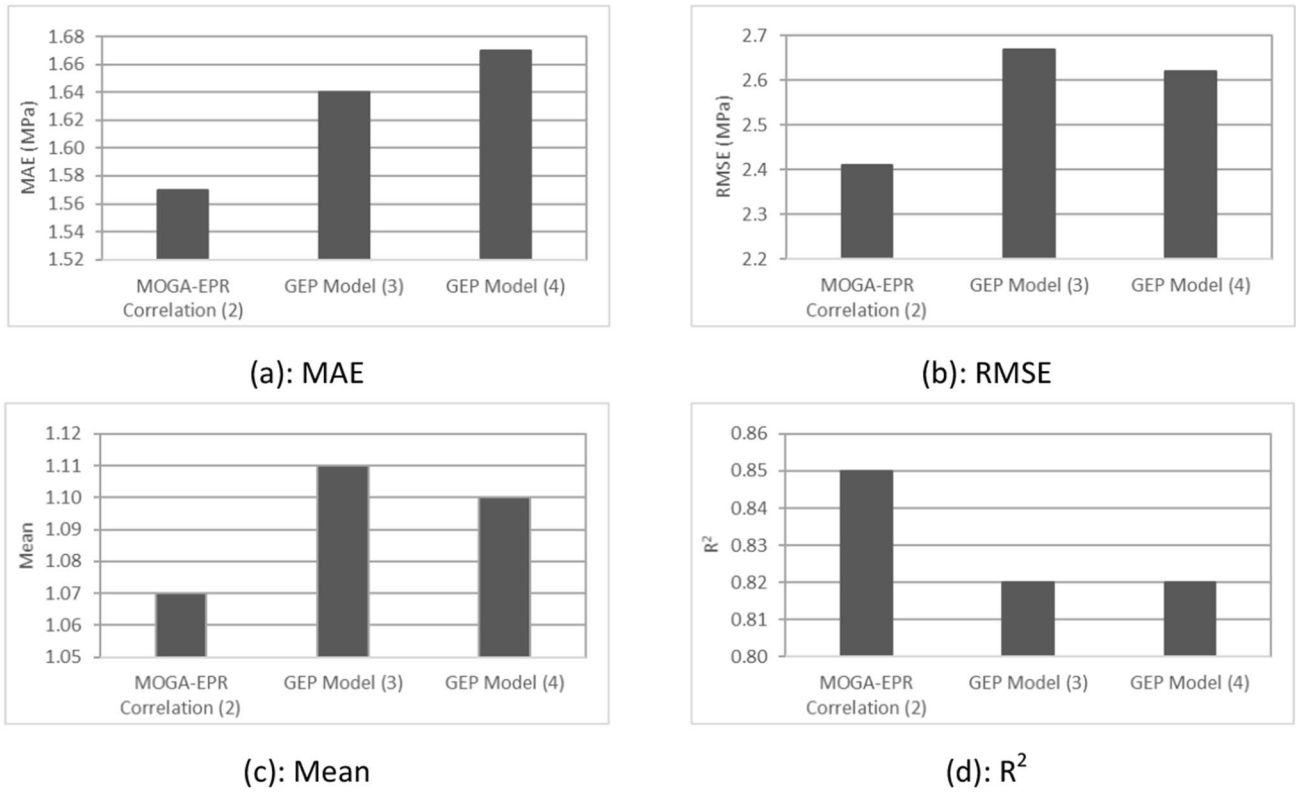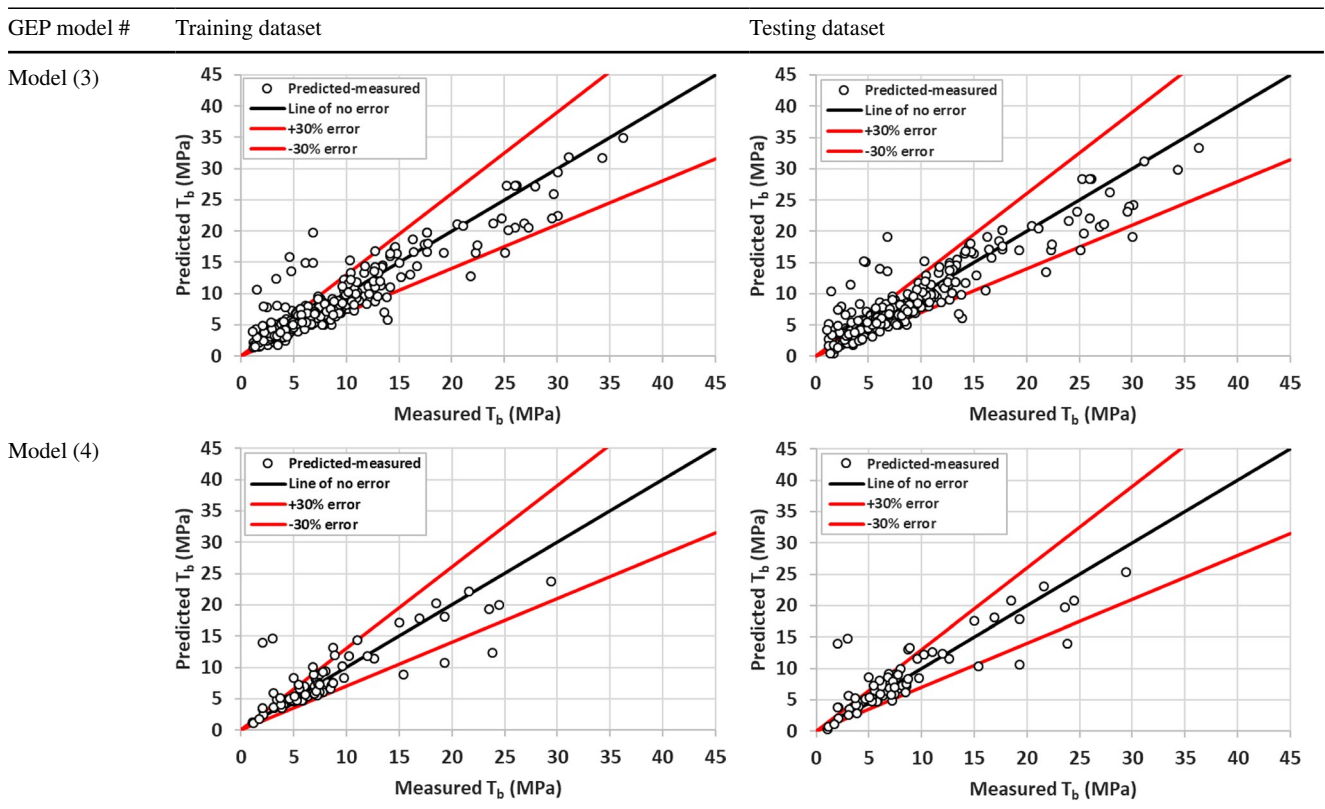
(a): MAE

(b): RMSE

(c): Mean

(d): R^2

Fig. 6 The Statistical indicators of the MOGA-EPR and developed models for all datasets for Correlation (2)

Table 17 Relationship between measured and predicted T_b in MPa using the GEP-developed models for the training and testing datasets for Correlation (2)

GEP model #	Training dataset	Testing dataset
Model (3)		
Model (4)		

Table 18 Statistical measures of the testing and training datasets for Correlation (3)

Statistical indicators	Training data			Testing data		
	MOGA-EPR Correlation (3)	GEP Model (5)	GEP Model (6)	MOGA-EPR Correlation (3)	GEP Model (5)	GEP Model (6)
MAE (MPa)	1.89	1.51	1.82	1.71	1.61	1.78
RMSE (MPa)	2.80	2.40	2.88	2.78	2.71	2.99
Mean (μ)	1.07	1.05	1.12	1.12	1.10	1.14
R^2	0.81	0.86	0.80	0.77	0.79	0.74
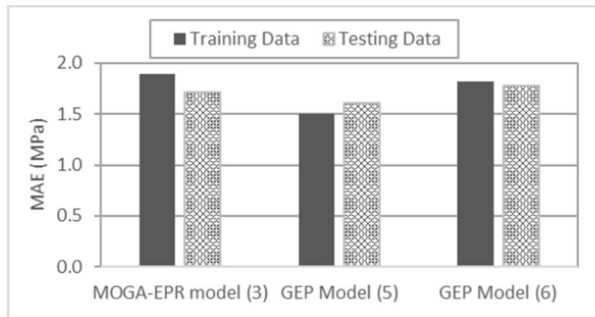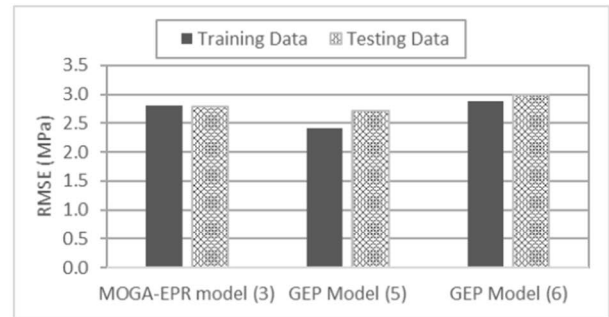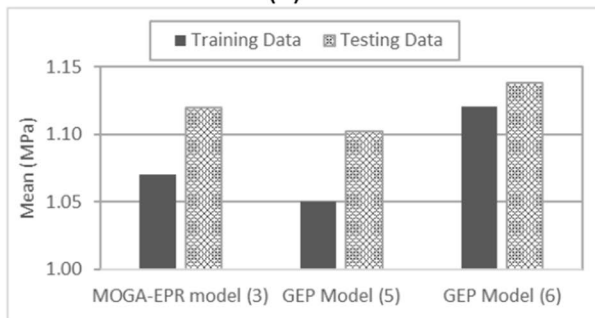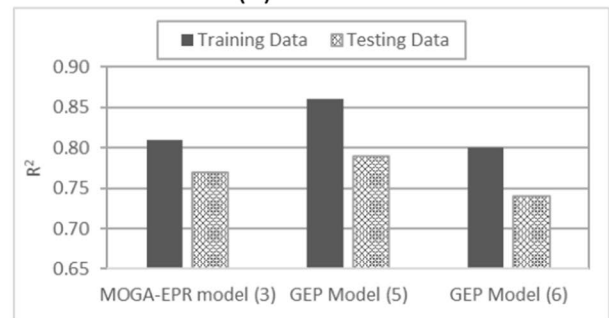
Fig. 7 The Statistical indicators of the developed models for both datasets for Correlation (3)

Table 19 Statistical measures of all datasets for Correlation (3)

Statistical measure/ Approach	MOGA-EPR correlation (3)	GEP model (5)	GEP model (6)
MAE (MPa)	1.86	1.53	1.81
RMSE (MPa)	2.80	2.47	2.90
Mean (μ)	1.08	1.06	1.12
R^2	0.80	0.84	0.79

increased porosity also increases the amount of water and other liquids that can be absorbed by the concrete, which in turn increases the bond strength. Additionally, aging increases the compressive strength of the concrete, which further increases the bond strength.

As shown in Fig. 9c, the effect of the failure surface temperature of concrete (T) on the bond between steel rebar and concrete (T_b) is studied, and it can be seen that as the temperature increases, the T_b decreases. This result corroborates the findings of reference [3], which
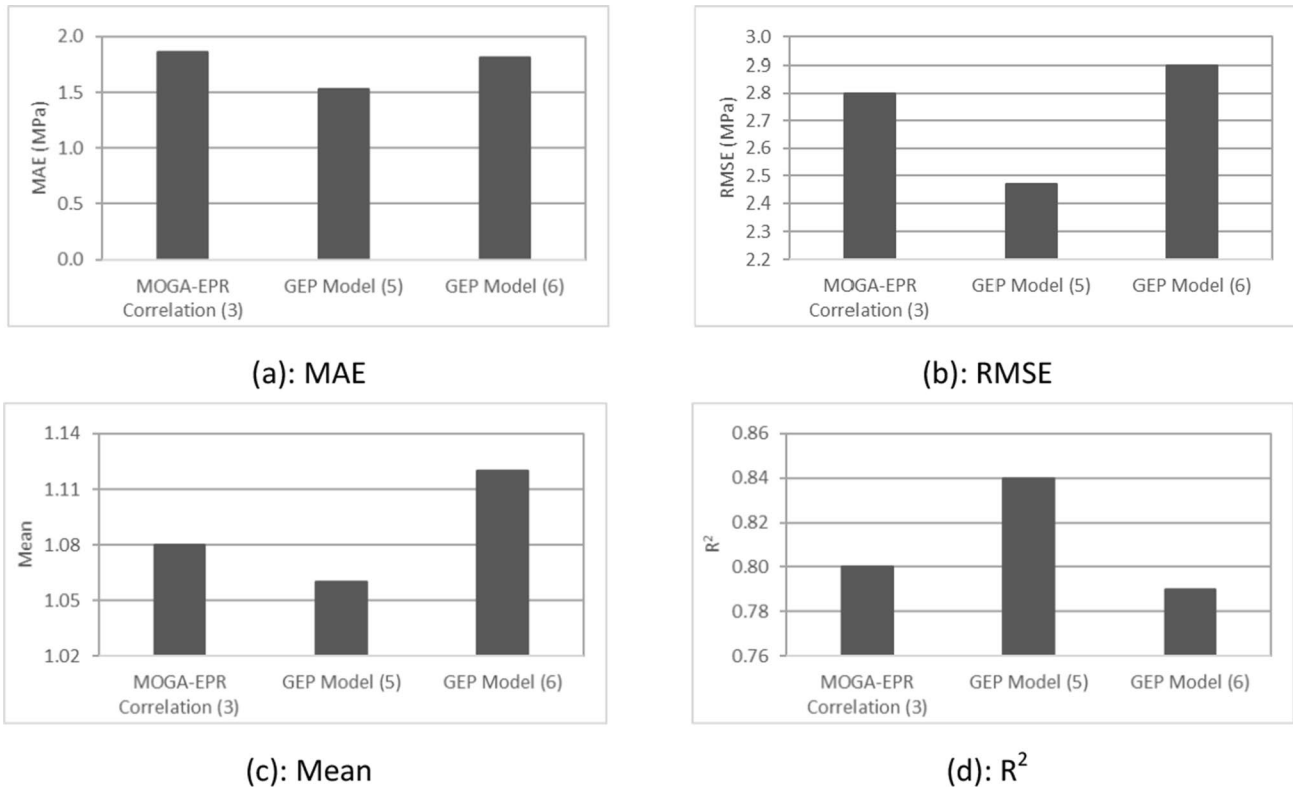
Fig. 8 The Statistical indicators of the MOGA-EPR and developed models for all datasets for Correlation (3)

suggests that when exposed to high temperatures, the bond between the two materials is significantly weakened due to the reduced strength of the concrete and potential plastic deformation of the embedded steel rebar. This bond degradation can have a major impact on the structural integrity of an RC component.

Conclusions

This research investigated the influence of elevated temperatures on the bond strength between concrete and steel (T_b) utilizing the GEP data-driven model. Six correlations to predict the bond strength were generated using the GEP approach and examined against the literature. A sensitivity analysis was executed to evaluate the effect of varying parameters on the bond strength. Based on the limitations of this study, the following conclusions can be made:

- Table 21 summarises the most accurate prediction equations for each correlation model. And shows that:

- For Correlation (1), the MOGA-EPR model has a higher R^2 of 0.85, compared to GEP models 1 and 2, which are 0.83 and 0.82, respectively.
- For Correlation (2), the MOGA-EPR model has a higher R^2 of 0.85, compared to the GEP models which is 0.82.
- For Correlation (3), the GEP model (5) has a higher R^2 of 0.84, compared to the MOGA-EPR model which is 0.8.

This indicates that all variables are incorporated in the Correlation (1) models to achieve the optimal fit, but it should be noted that the Correlations (2) and (3) models remain valid.

- The sensitivity study examined the influence of changing the ratio of the period of thermal saturation at the maximum desired temperature to the minimal size of the extracted sample (Δ), age of testing (A), and failure surface temperature of concrete (T) on the bond between the concrete and steel (T_b). The results of the analysis were summarized as:

Table 20 Relationship between measured and predicted T_b in MPa using the GEP-developed models for the training and testing datasets for Correlation (3)

GEP model #	Training dataset	Testing dataset
Model (5)		
Model (6)		
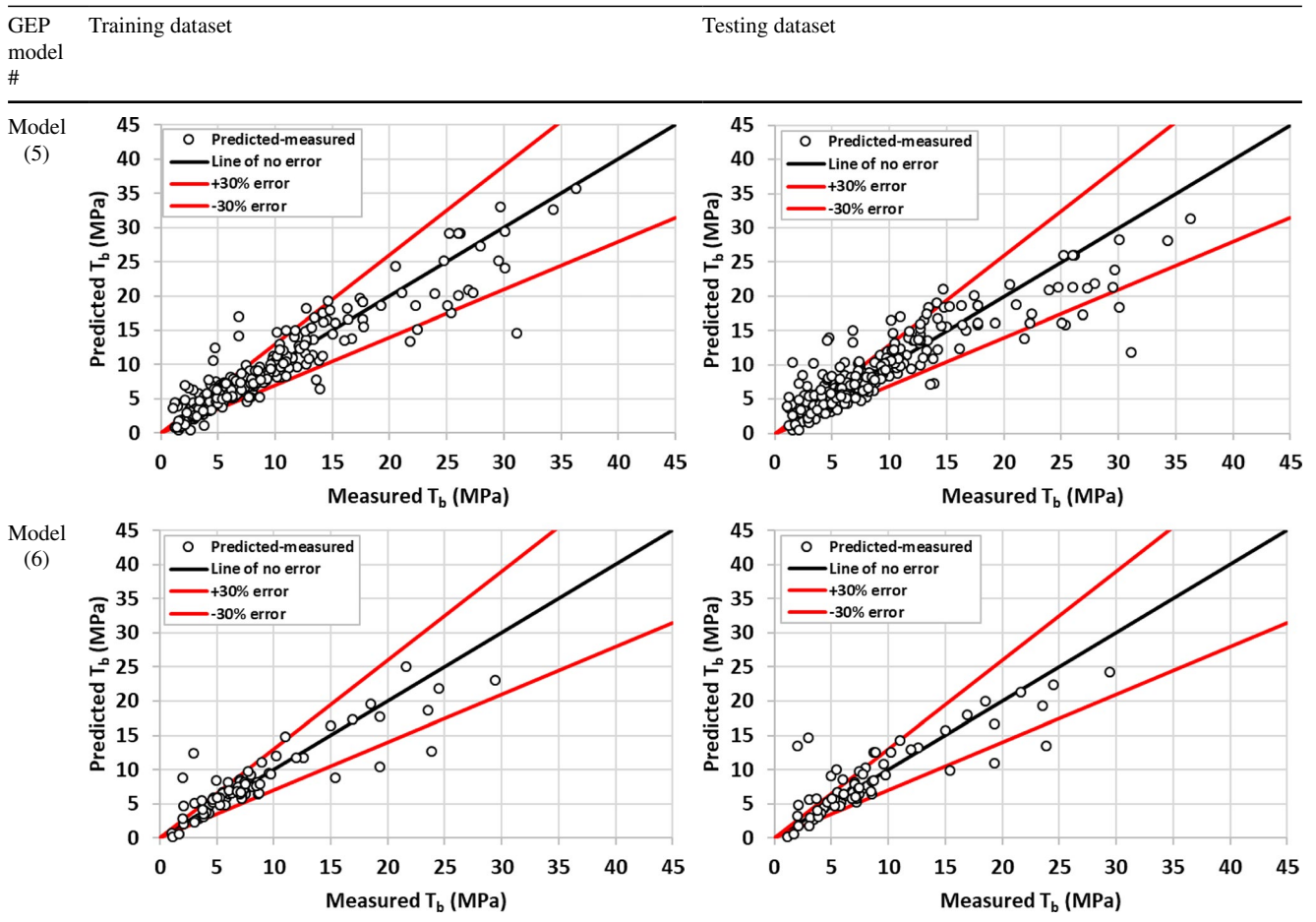
- The bond between steel rebar and concrete (T_b) decreases as its thermal saturation ratio Δ increases.
- Increasing concrete age (A) leads to a higher bond between steel rebar and concrete (T_b).
- The steel rebar and concrete (T_b) bond decreases with a temperature rise.

This research provides insights into how concrete-steel bond performance is affected by the Age of Testing under high temperatures. This knowledge can be beneficial in the creation of further studies and the making of design decisions in the future.

As a future work, it would be beneficial to explore and optimize the value of the number of chromosomes and use different setting parameters in GEP models, considering the limitations observed in this paper. Currently, a fixed number of chromosomes and setting parameters are utilized, but it is essential to acknowledge that increasing the number of chromosomes can potentially lead to heightened computational complexity and longer computation durations. Additionally, a larger population size might be necessary to maintain a satisfactory level of diversity. Therefore, it is crucial to strike a balance between exploration and exploitation while determining the appropriate number of chromosomes, taking into account the demand for diversity, available computational resources, and the complexity of the problem. To address this, future research should conduct a more comprehensive analysis to investigate and optimize the value of this parameter. By doing so, the effect of these parameters on the accuracy and reliability of the research outcomes can be studied, thereby enhancing the understanding and application of GEP models.
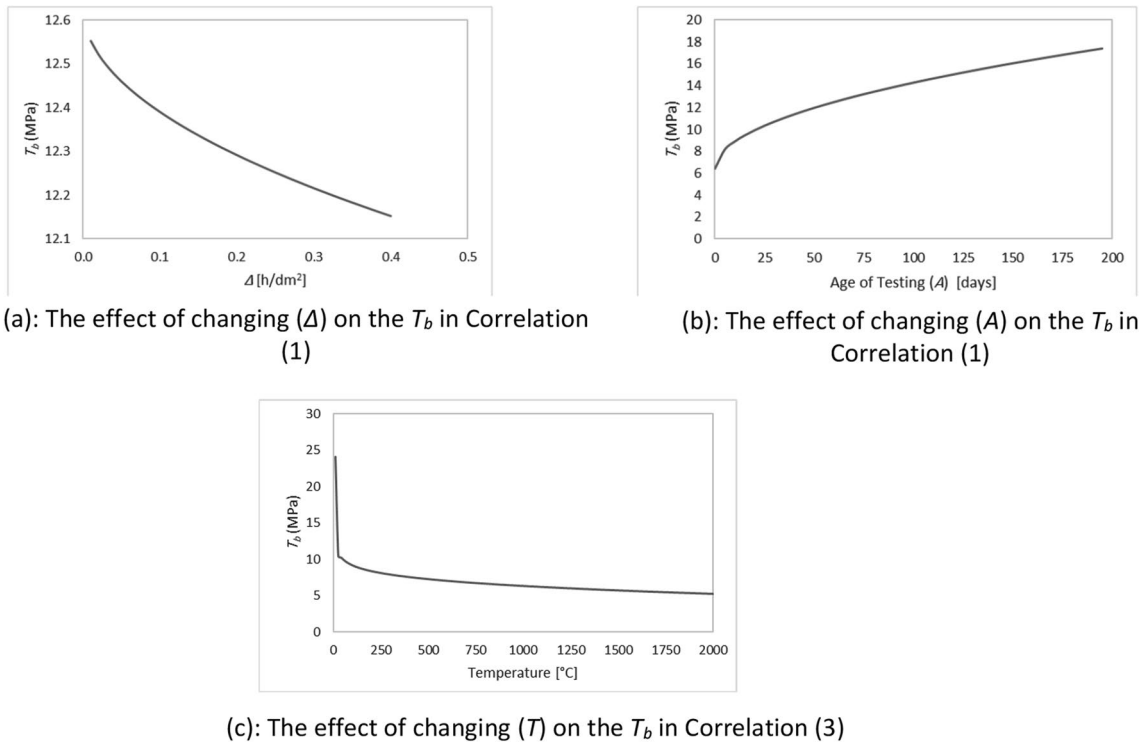
(a): The effect of changing (Δ) on the T_b in Correlation (1)

(b): The effect of changing (A) on the T_b in Correlation (1)

(c): The effect of changing (T) on the T_b in Correlation (3)

Fig. 9 Sensitivity Studies on the T_b

Table 21 The most accurate models for the different correlations

Correlation #	Model #	Predicted T_b equation	Coefficients	Equation #
(1)	MOGA-EPR Correlation (1)	$T_{batfailure} = a_1 \times \sqrt{c/d} \times \sqrt{A} \times f_c$ $+ a_2 \times c/d \times f_c \times T^2 + a_3 \times \sqrt{l/d} \times \sqrt{A} \times f_c$ $+ a_4 \times \sqrt{V} \times \sqrt{\Delta} \times (c/d) \times T^2$ $+ a_5 \times \sqrt{l/d} \times \sqrt{V} \times (c/d) + a_6$	$a_1 = 3.59 \times 10^{-2}$ $a_2 = -7.5 \times 10^{-8}$ $a_3 = -1.68 \times 10^{-2}$ $a_4 = -3.5 \times 10^{-6}$ $a_5 = 8.48 \times 10^{-1}$ $a_6 = 4.047$	(4)
(2)	MOGA-EPR Correlation (2)	$T_{batfailure} = b_1 \times c/d \times f_c \times T^2$ $+ b_2 \times c/d \times f_c \times \sqrt{A} + b_3 \times (c/d)^2 \times f_c^2 \times \sqrt{A}$ $+ b_4 \times \sqrt{l/d} \times \sqrt{c/d} \times \sqrt{A} \times f_c$ $+ b_5 \times V \times f_c \times (c/d)^2 + b_6$	$b_1 = -1.12 \times 10^{-7}$ $b_2 = 2.3 \times 10^{-2}$ $b_3 = -1.8 \times 10^{-5}$ $b_4 = -8.7 \times 10^{-3}$ $b_5 = 1.05 \times 10^{-2}$ $b_6 = 2.789$	(5)
(3)	Model (5)	$T_{batfailure} = c/d + h_1 + (\frac{h_2}{h_3} \times \frac{V}{T} \times (T - l/d))$ $+ \frac{(c/d + f_c - \frac{f_c}{c/d}) \times (\frac{c/d}{l/d} + c/d)}{(c/d \times l/d) - V - h_4} + 2h_5 + (\frac{c/d^2 \times V}{T} \times (c/d + h_6))$ $+ \frac{T}{(h_7 + l/d) \times (h_8 - V) \times (h_9 \times c/d^2)} + \frac{h_{10} - T - 2c/d}{h_{11} - c/d - c/d^2}$	$h_1 = 6.72220138634907$ $h_2 = -9.83733063127537$ $h_3 = -8.96069493697928$ $h_4 = 2.36795561174352$ $h_5 = -3.31615874279132$ $h_6 = -9.81580553605762$ $h_7 = -3.49237127774238$ $h_8 = -8.07519140742794$ $h_9 = -3.64402905362102$ $h_{10} = 9.94811416994824$ $h_{11} = 210.77762807679$	(11)

Declarations

Conflict of interest None declared.

Ethical approval The authors state that the research was conducted according to ethical standards.

Informed consent For the type of this study formal consent not required.

References

1. EN1992–1–2–2004, Eurocode 2: Design of concrete structures—Part 1–2: General rules: Structural fire design, in: Eurocode 2, 2004 https://archive.org/details/en.1992.1.2.2004

2. CEB-FIP International Federation for Structural Concrete, fib Model Code 2010, (2013) fédération internationale du béton/International federation for structural concrete (fib) Postal, Lausanne, Switzerland, Switzerland, 2010.

3. Diederichs U, Schneider U (1981) Bond strength at high temperatures. Mag Concr Res 33:75–84. https://doi.org/10.1680/macr.1981.33.115.75

4. Khan MR (1986) Post heat exposure behaviour of reinforced concrete beams. Mag Concr Res 38:59–66. https://doi.org/10.1680/macr.1986.38.135.59

5. Yang O, Zhang B, Yan G, Chen J (2018) Bond performance between slightly corroded steel bar and concrete after exposure to high temperature. J Struct Eng 144:04018209. https://doi.org/10.1061/(asce)st.1943-541x.0002217

6. Varona FB, Baeza FJ, Bru D, Ivorra S, Villacampa Y, Navarro-González FJ, Bru D, Baeza FJ (2019) Non-linear multivariable model for predicting the steel to concrete bond after high temperature exposure. Constr Build Mater 249:118713. https://doi.org/10.2495/CMEM190191

7. Varona FB, Baeza FJ, Bru D, Ivorra S (2018) Evolution of the bond strength between reinforcing steel and fibre reinforced concrete after high temperature exposure. Constr Build Mater 176:359–370. https://doi.org/10.1016/j.conbuildmat.2018.05.065

8. Varona FB, Baeza FJ, Ivorra S, Bru D (2015) Experimental analysis of the loss of bond between rebars and concrete exposed to high temperatures | Análisis experimental de la pérdida de adherencia hormigón-acero en hormigones sometidos a altas temperaturas. Dyna Spain 90:78–86. https://doi.org/10.6036/7184

9. F.B. Varona, F.J. Baeza, D. Bru, S. Ivorra, Database of experimental results for steel-to-concrete bond at high temperature. Mandeley Data 2, 585263 DOI: https://doi.org/10.17632/CVB6BMCPMK.2.

10. Mousavi A, Hajiloo H, Green MF (2021) Bond performance of GFRP reinforcing bars under uniform or gradient temperature distributions. J Compos Constr. https://doi.org/10.1061/(asce)cc.1943-5614.0001169

11. Al-Hamd RKS, Gillie M, Mohamad SA, Cunningham LS (2020) Influence of loading ratio on flat slab connections at elevated temperature: a numerical study. Front Struct Civ Eng 14:664–674. https://doi.org/10.1007/s11709-020-0620-9

12. Bazant ZP, Kaplan MF (1996) Concrete at high temperatures: material properties and mathematical models.

13. Foti D (2014) Prestressed slab beams subjected to high temperatures. Compos Part B Eng 58:83. https://doi.org/10.1016/j.compositesb.2013.10.083

14. Bailey CG, Ellobody E (2009) Whole-building behaviour of bonded post-tensioned concrete floor plates exposed to fire. Eng Struct 31:33. https://doi.org/10.1016/j.engstruct.2009.02.033

15. Al-Hamd RKS, Gillie M, Wang Y (2017) Numerical modelling of slab-column concrete connections at elevated temperatures. IABSE Sympos Rep 109:3365–3369. https://doi.org/10.2749/222137817822208528

16. Al Hamd RKhS, Gillie M, Warren H, Torelli G, Stratford T, Wang Y (2018) The effect of load-induced thermal strain on flat slab behaviour at elevated temperatures. Fire Saf J 97:12–18. https://doi.org/10.1016/j.firesaf.2018.02.004

17. Al-Hamd RKS, Gillie M, Cunningham LS, Warren H, Albostami AS (2019) Novel shearhead reinforcement for slab-column connections subject to eccentric load and fire. Arch Civ Mech Eng 19:503–524. https://doi.org/10.1016/j.acme.2018.12.011

18. Ahmed AE, Al-Shaikh AH, Arafat TI (1992) Residual compressive and bond strengths of limestone aggregate concrete subjected to elevated temperatures. Magaz Concr Res 44:117. https://doi.org/10.1680/macr.1992.44.159.117

19. Naser MZ (2021) An engineer's guide to explainable artificial intelligence and interpretable machine learning: navigating causality, forced goodness, and the false perception of inference. Autom Constr. https://doi.org/10.1016/j.autcon.2021.103821

20. Ahangar-Asr A, Javadi AA, Johari A, Chen Y (2014) Lateral load bearing capacity modelling of piles in cohesive soils in undrained conditions: an intelligent evolutionary approach. Appl Soft Comput J. https://doi.org/10.1016/j.asoc.2014.07.027

21. Ahangar Asr A, Faramarzi A, Javadi AA (2018) An evolutionary modelling approach to predicting stress-strain behaviour of saturated granular soils. Eng Comput Swansea Wales. https://doi.org/10.1108/EC-01-2018-0025

22. Alzabeebee S (2020) Dynamic response and design of a skirted strip foundation subjected to vertical vibration. Geomech Eng. https://doi.org/10.12989/gae.2020.20.4.345

23. Alzabeebee S, Chapman DN, Faramarzi A (2018) Development of a novel model to estimate bedding factors to ensure the economic and robust design of rigid pipes under soil loads. Tunn Undergr Space Technol. https://doi.org/10.1016/j.tust.2017.11.009

24. Alzabeebee S, Chapman DN, Faramarzi A (2019) Economical design of buried concrete pipes subjected to UK standard traffic loading. Proc Inst Civ Eng Struct Build. https://doi.org/10.1680/jstbu.17.00035

25. Shams MA, Shahin MA, Ismail MA (2020) Design of stiffened slab foundations on reactive soils using 3D numerical modeling. Int J Geomech. https://doi.org/10.1061/(asce)gm.1943-5622.0001654

26. Du Z, Shahin MA, El Naggar H (2021) Design of ram-compacted bearing base piling foundations by simple numerical modelling approach and artificial intelligence technique. Int J Geosynth Ground Eng. https://doi.org/10.1007/s40891-021-00287-6

27. Nassr A, Esmaeili-Falak M, Katebi H, Javadi A (2018) A new approach to modeling the behavior of frozen soils. Eng Geol. https://doi.org/10.1016/j.enggeo.2018.09.018

28. Nassr A, Javadi A, Faramarzi A (2018) Developing constitutive models from EPR-based self-learning finite element analysis. Int J Numer Anal Meth Geomech. https://doi.org/10.1002/nag.2747

29. Alzabeebee S, Al-Hamd RKS, Nassr A, Kareem M, Keawsawasvong S (2023) Multiscale soft computing-based model of shear strength of steel fibre-reinforced concrete beams. Innov Infrastruct Solut 8:1028. https://doi.org/10.1007/s41062-022-01028-y

30. Albostami AS, Al-Hamd RKhS, Alzabeebee S, Minto A, Keawsawasvong S (2023) Application of soft computing in predicting the compressive strength of self-compacted concrete containing recyclable aggregate. Asian J Civil Eng. https://doi.org/10.1007/s42107-023-00767-2

31. DeRousseau MA, Kasprzyk JR, Srubar WV (2018) Computational design optimization of concrete mixtures: a review. Cem Concr Res 109:42–53. https://doi.org/10.1016/j.cemconres.2018.04.007

32. Tong Z, Huo J, Wang Z (2020) High-throughput design of fiber reinforced cement-based composites using deep learning. Cem Concr Compos 113:103716. https://doi.org/10.1016/j.cemconcomp.2020.103716

33. Zhang J, Huang Y, Ma G, Sun J, Nener B (2020) A metaheuristic-optimized multi-output model for predicting multiple properties of pervious concrete. Construct Build Mater 249:118803. https://doi.org/10.1016/j.conbuildmat.2020.118803

34. Kaloop MR, Kumar D, Samui P, Hu JW, Kim D (2020) Compressive strength prediction of high-performance concrete using gradient tree boosting machine. Construct Build Mater 264:120198. https://doi.org/10.1016/j.conbuildmat.2020.120198

35. Ford E, Kailas S, Maneparambil K, Neithalath N (2020) Machine learning approaches to predict the micromechanical properties of cementitious hydration phases from microstructural chemical maps. Construct Build Mater 265:120647. https://doi.org/10.1016/j.conbuildmat.2020.120647

36. Han Q, Gui C, Xu J, Lacidogna G (2019) A generalized method to predict the compressive strength of high-performance concrete by improved random forest algorithm. Constr Build Mater 226:734–742. https://doi.org/10.1016/j.conbuildmat.2019.07.315

37. Ramkumar KB, Kannan Rajkumar PR, Noor Ahmmad S, Jegan M (2020) A review on performance of self-compacting concrete—use of mineral admixtures and steel fibres with artificial neural network application. Construct Build Mater 261:120251. https://doi.org/10.1016/j.conbuildmat.2020.120215

38. Hendi A, Mostofinejad D, Sedaghatdoost A, Zohrabi M, Naeimi N, Tavakolinia A (2019) Mix design of the green self-consolidating concrete: incorporating the waste glass powder. Constr Build Mater 199:369–384. https://doi.org/10.1016/j.conbuildmat.2018.12.020

39. Nunez I, Nehdi ML (2021) Machine learning prediction of carbonation depth in recycled aggregate concrete incorporating SCMs. Construct Build Mater 287:123027. https://doi.org/10.1016/j.conbuildmat.2021.123027

40. Xu J, Zhao X, Yu Y, Xie T, Yang G, Xue J (2019) Parametric sensitivity analysis and modelling of mechanical properties of normal- and high-strength recycled aggregate concrete using grey theory, multiple nonlinear regression and artificial neural networks. Constr Build Mater 211:479–491. https://doi.org/10.1016/j.conbuildmat.2019.03.234

41. Li Z, Yoon J, Zhang R, Rajabipour F, Srubar WV, Dabo I, Radlińska A (2022) Machine learning in concrete science: applications, challenges, and best practices. NPJ Comput Mater 8:810. https://doi.org/10.1038/s41524-022-00810-x

42. Al Hamd RKS, Alzabeebee S, Cunningham LS, Gales J (2022) Bond behaviour of rebar in concrete at elevated temperatures: a soft computing approach. Fire Mater. https://doi.org/10.1002/fam.3123

43. Ferreira C (2001) Gene expression programming: a new adaptive algorithm for solving problems. Complex Syst 13:87–129

44. Faradonbeh R, Armaghani D, Abd Majid MZ, Tahir MMD, Ramesh Murlidhar B, Monjezi M, Wong HM (2016) Prediction of ground vibration due to quarry blasting based on gene expression programming: a new model for peak particle velocity prediction. Int J Environ Sci Technol 13:1453–1464. https://doi.org/10.1007/s13762-016-0979-2

45. A.H. Gandomi Amir, H. Alavi Conor, R. Eds (2015) Handbook of genetic programming applications, Springer, Cham.

46. Koza JR (1992) Genetic programming: on the programming of computers by means of natural selection. MIT Press, Cambridge

47. Ferreira C (2006) Gene expression programming: mathematical modeling by an artificial intelligence. Springer

48. Alkroosh IS, Bahadori M, Nikraz H, Bahadori A (2015) Regressive approach for predicting bearing capacity of bored piles from cone penetration test data. J Rock Mech Geotech Eng 7:584–592. https://doi.org/10.1016/j.jrmge.2015.06.011

49. Kordnaeij A, Kalantary F, Kordtabar B, Mola-Abasi H (2015) Prediction of recompression index using GMDH-type neural network based on geotechnical soil properties. Soils Found 55:1335–1345. https://doi.org/10.1016/j.sandf.2015.10.001

50. Huang CF, Li Q, Wu SC, Liu Y, Li J-Y (2019) Assessment of empirical equations of the compression index of muddy clay: sensitivity to geographic locality. Arab J Geosci 12:4275. https://doi.org/10.1007/s12517-019-4276-5

51. Tinoco J, Alberto A, da Venda P, Gomes Correia A, Lemos L (2020) A novel approach based on soft computing techniques for unconfined compression strength prediction of soil cement mixtures. Neural Comput Appl 32:8985–8991. https://doi.org/10.1007/s00521-019-04399-z

52. Zhang W, Zhang R, Wu C, Goh ATC, Lacasse S, Liu Z, Liu H (2020) State-of-the-art review of soft computing applications in underground excavations. Geosci Front 11:1095–1106. https://doi.org/10.1016/j.gsf.2019.12.003